Supplementary Information

Molecular dipole engineering assisted strain release for mechanically robust flexible perovskite solar cells

Lisha Xie[†ab], Songyu Du[†ab], Jun Li[†ab], Chang Liu[ab], Zhenwei Pu[ab], Xinyu Tong[ab], Jian Liu[ab], Yaohua Wang[ab], Yuanyuan Meng[ab], Mengjin Yang[ab], Wei Li*[ab] and Ziyi Ge*[ab]

[a]Zhejiang Provincial Engineering Research Center of Energy Optoelectronic Materials and Devices, Ningbo Institute of Materials Technology and Engineering, Chinese Academy of Sciences, Ningbo 315201, P. R. China.
E-mail: liwei1987@nimte.ac.cn, geziyi@nimte.ac.cn.

[b]Center of Materials Science and Optoelectronics Engineering, University of Chinese Academy of Sciences, Beijing, 100049, P. R. China.

* Corresponding authors.

† Contributed equally to this work.

Experimental

Materials and solvents

For this work, [2-(3,6-dimethoxy-9H-carbazol-9-yl)ethyl]phosphonic acid (MeO-2PACz, 98.0%), N,N-dimethylformamide (DMF, 99.8%), and dimethyl sulfoxide (DMSO, 99.8%) were purchased from Tokyo Chemical Industry Co., Ltd. (TCI). Acetone (98%) and diethyl ether (99.7%) were purchased from Sinopharm Chemical Reagent Co., Ltd. Isopropanol (IPA, 99.7%) and ethanol (99.5%) were purchased from General Reagent.

Methylammonium chloride (MACl, 99.9%), methylammonium bromide (MABr, 99.99%), formamidinium iodide (FAI, 99.99%), cesium iodide (CsI, 99.9%), lead(II) iodide (PbI_2, 99.99%), lead(II) bromine ($PbBr_2$, 99.999%), buckminsterfullerene (C_{60}, 99.99%), and bathocuproine (BCP, 99.9%) were purchased from Advanced Election Technology Co., Ltd.

Preparation of control and modified perovskite precursor solution

A total of 3.68 mg MABr, 276.98 mg FAI, 18.11 mg MACl, 12.70 mg $PbBr_2$, 22.47 mg CsI, and 821.47 mg PbI_2 were dissolved in 833 μL DMF and 167 μL DMSO solution, and stirred at room temperature overnight to prepare the undoped precursor solution. For the doped solution, another 1 mg each of 1F-2CN, 2F-2CN, and 3F-2CN was added in the previous solution.

Device fabrication

The inverted device architecture was PEN(ITO)/MeO-2PACz/PSK/C_{60}/BCP/Ag. The PEN(ITO) substrate was treated with UV-ozone for 15 min without cleaning. MeO-2PACz with a concentration of 0.3 mg/mL in IPA was spin-coated at 4000 rpm for 30 s onto treated ITO substrates and annealed at 100 ℃ for 10 min to fabricate the hole selection layer. The as-prepared perovskite precursor solution was spin-coated onto the modified HTL substrate at 1000 and 5000 rpm for 10 and 40 s, respectively. During the last 20 s of the spinning process, the film was treated by drop-casting diethyl ether (450 μL). The substrates were annealed on a hot plate at 100 °C for 30 min. Then, 25 nm thick C_{60}, 6 nm thick BCP, and 100 nm thick Ag were deposited on the top layer-wise via thermal evaporation.

Characterization

The 1H and 13C NMR spectra were recorded on Bruker (AVANCE III 600 MHz). The XPS spectra were determined using a monochromatic Al-Ka (1486.6 eV) radiation source (Shimadzu, Axis Supra). The top-view morphologies were recorded on Gemini SEM 300 and Dimension ICON SPM. Dimension ICON SPM was also used to obtain the Young's modulus and c-AFM. The energy level was determined via UPS (R3000, Scienta) with HeI (21.2 eV) as the excitation source and UV-vis spectroscopy (Lambda 950). The X-ray diffraction (XRD) experiment was performed using Mini Flex 600 (Rigaku, Japan). Depth-resolved GIXRD measurements were performed using a Rigaku SmartLab five-axis X-ray diffractometer at 45 kV and 200 mA with Cu Kα radiation (λ = 1.54050 Å). The temperature-dependent PL spectra, steady-state PL, and TRPL decay spectra were measured using a fluorescence spectrometer (FLS 980) with a 450 nm laser (EPL-510, Edinburgh Instruments Ltd.). Femtosecond TAS was performed using SOL-F-K-HP-T at 400 nm. The *J-V* characteristics were measured using a solar simulator (San-EI Electric) with standard AM 1.5G (100 mW cm^{-2}) illumination and Keithley 2400 source. The light intensity was calibrated using a standard silicon solar cell, AK-200 (Konica Minolta). EQE data were obtained using QE-R (Enlitech).

Note 1: Strain[1-3]

According to Bragg's law and generalized Hooke's law, the residual strain can be calculated as the slope of the following function:

$$\sigma = -\frac{E}{2(1+\nu)}\frac{\pi}{180^\circ}cot\theta_0\frac{\partial(2\theta)}{\partial sin^2\varphi}$$

where φ, E, 2θ, θ_0, and ν represent the angle of diffraction vector corresponding to the sample surface normal, perovskite modulus, scattering angle of the actual perovskite, half of the scattering angle ($2\theta_0$) corresponding to a given diffraction peak for stress-free perovskite, and Poisson's ratio of the perovskite, respectively.

Note 2: TRPL/TAS[4]

The TRPL/TAS decay curves were fitted by the following bi-exponential function:

$$f(t) = A_1 e^{\frac{-t}{\tau_1}} + A_2 e^{\frac{-t}{\tau_2}} + B$$

$$\tau_{ave} = \frac{A_1 {\tau_1}^2 + A_2 {\tau_2}^2}{A_1 \tau_1 + A_2 \tau_2},$$

where τ_1 represents the short transient lifetime, τ_2 represents the long transient lifetime, A_1 and A_2 are constants, and B is the baseline offset constant.

Note 3: Electron–phonon coupling[5-7]

The electron-phonon coupling was calculated by the Bose-Einstein thermal distribution equation:

$$\Gamma(T) = \Gamma_{\text{inh}} + \frac{\Gamma_{\text{LO}}}{e^{\frac{h\omega}{k_B T}} - 1}$$

where Γ_{inh} is the inhomogeneous line width due to structural disorder, Γ_{LO} is the electron-LO phonon coupling coefficient, and $h\omega$ represents the LO phonon energy.

Note 4: SCLC[8, 9]

The trap densities (N_t) of the perovskite films were calculated using the following equation:

$$N_t = \frac{2V_{TFL}\varepsilon_0\varepsilon_r}{eL^2},$$

where e, L, ε_0, and ε_r represent the electron charge, thickness of perovskite film, vacuum permittivity, and relative dielectric constant of perovskite, respectively.

Synthesis

All reagents were purchased from the Casmart Reagent Platform and used as received without further purification. All compounds were synthesized via one-step common palladium-catalyzed Suzuki coupling reactions of *5*-bromoisophthalonitrile (**2CN-Br**) and corresponding boric acid-functionalized fragments. The synthesis process was showed in detail below.

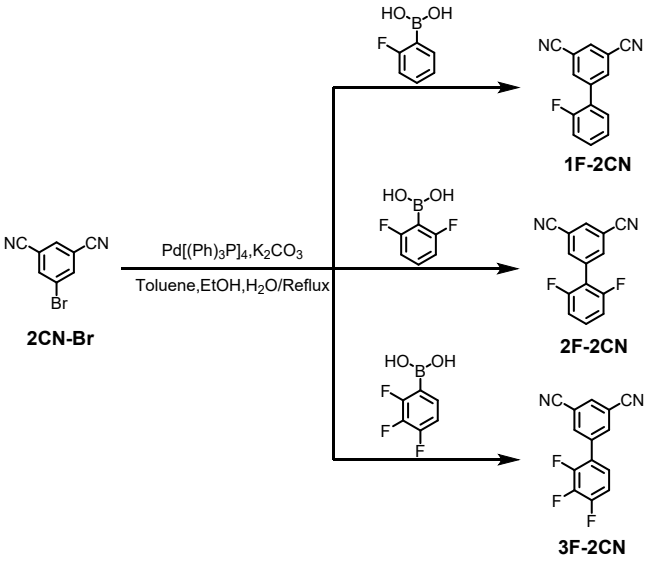

Schemes S1. Chemical structures and synthetic routes for **1F-2CN**, **2F-2CN**, and **3F-2CN**.

Synthesis of 2'-fluoro-[1,1'-biphenyl]-3,5-dicarbonitrile (1F-2CN):

2CN-Br (2.06 g, 10 mmol), (*2*-fluorophenyl)boronic acid (1.54g, 10 mmol), $Pd(P(Ph)_3)_4$ (0.57 g, 0.5 mmol), 4.44 mmol), K_2CO_3 (6.90 g, 50 mmol) were dissolved in 120 mL toluene and 30 mL EtOH in a 250 mL three-necked flask. The mixture was continuously stirred at 90 ^oC for 8 hours under the nitrogen atmosphere. After cooling to room temperature, 200 mL of deionized water was added to the mixture. The reaction mixture was extracted with dichloromethane (3 x 100 mL), dried over anhydrous magnesium sulfate, and the solvent was removed under vacuum to give a red powder. The crude product was purified by column chromatography on silica gel (PE/DCM = 10:1, v/v). The product was further purified by sublimation and obtained 1.78 g white solid, yielding 80.1 %. ^1H NMR (400 MHz, Chloroform-*d*) δ 8.07 (d, *J* = 1.5 Hz, 2H), 7.93 (t, *J* = 1.6 Hz, 1H), 7.53 – 7.38 (m, 2H), 7.31 (td, *J* = 7.6, 1.2 Hz, 1H), 7.28 – 7.15 (m, 1H). ^{13}C NMR (151 MHz, $CDCl_3$) δ 138.73, 136.29, 136.26, 133.95, 131.52, 130.16, 125.22, 116.83, 116.68, 116.56, 114.47. TOF-MS (APCI) m/z, found: 222.0611, Calculated for $C_{14}H_7FN_2$: 222.0593.

Synthesis of compound 2',6'-difluoro-[1,1'-biphenyl]-3,5-dicarbonitrile (2F-2CN):

The reaction of intermediate ***2CN-Br*** with (2,6-fluorophenyl)boronic acid following the same procedure for the synthesis of ***1F-2CN*** generated the pure ***2F-2CN*** as a

white powder (yield:78 %). ^{1}H NMR (400 MHz, Chloroform-*d*) δ 8.01 (q, *J* = 1.4 Hz, 2H), 7.97 (d, *J* = 1.6 Hz, 1H), 7.44 (tt, *J* = 8.4, 6.3 Hz, 1H), 7.08 (t, *J* = 8.2 Hz, 2H). ^{13}C NMR (151 MHz, $CDCl_3$) δ 138.79, 137.69, 134.61, 133.77, 116.38, 115.64, 115.28, 114.44, 112.38. TOF-MS (APCI) m/z, found: 240.0513, Calculated for $C_{14}H_6F_2N_2$: 240.0499.

***Synthesis of compound 2',3',4'-trifluoro-[1,1'-biphenyl]-3,5-dicarbonitrile (3F-2CN)*:**

The reaction of intermediate ***2CN-Br*** with (2,3,4-trifluorophenyl)boronic acid following the same procedure for the synthesis of ***1F-2CN*** generated the pure ***2F-2CN*** as a white powder (yield:78 %). ^{1}H NMR (400 MHz, Chloroform-d) δ 8.01 (t, J = 1.4 Hz, 2H), 7.97 (t, J = 1.5 Hz, 1H), 7.16 (dd, J = 7.3, 5.1 Hz, 2H). ^{13}C NMR (151 MHz, $CDCl_3$) δ 136.94, 136.01, 135.99, 134.57, 123.69, 123.67, 123.65, 116.23, 114.87, 113.44, 113.32. TOF-MS (APCI) m/z, found: 258.0413, Calculated for: $C_{14}H_5F_3N_2$: 258.0405.

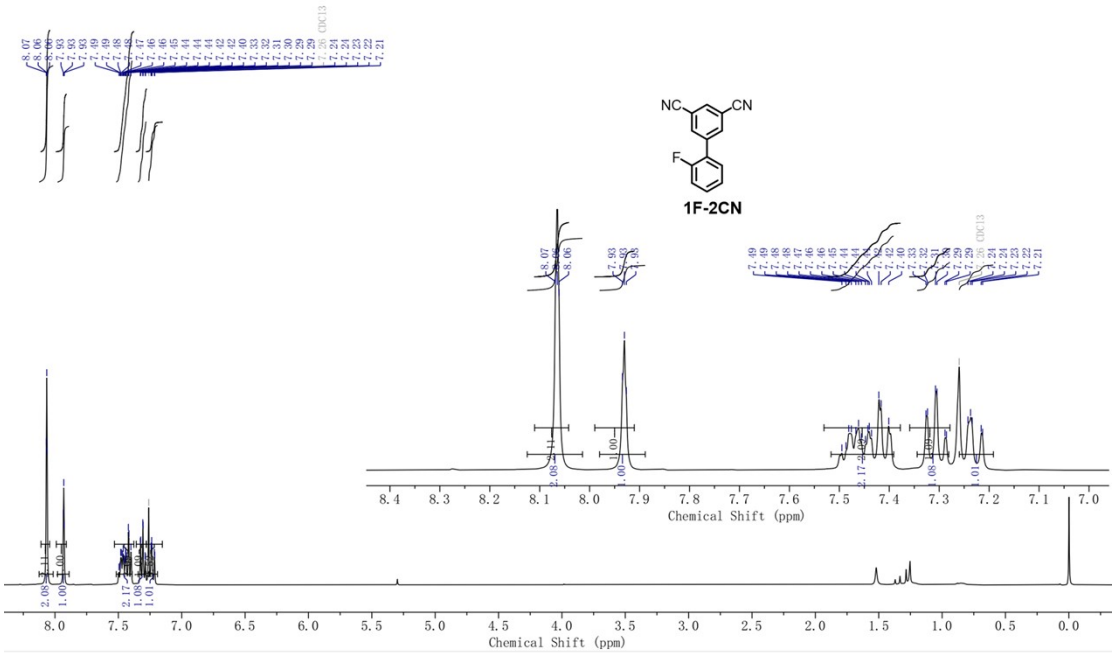

Fig. S1. ^{1}H NMR spectra of 1F-2CN in *d*-$CDCl_3$.

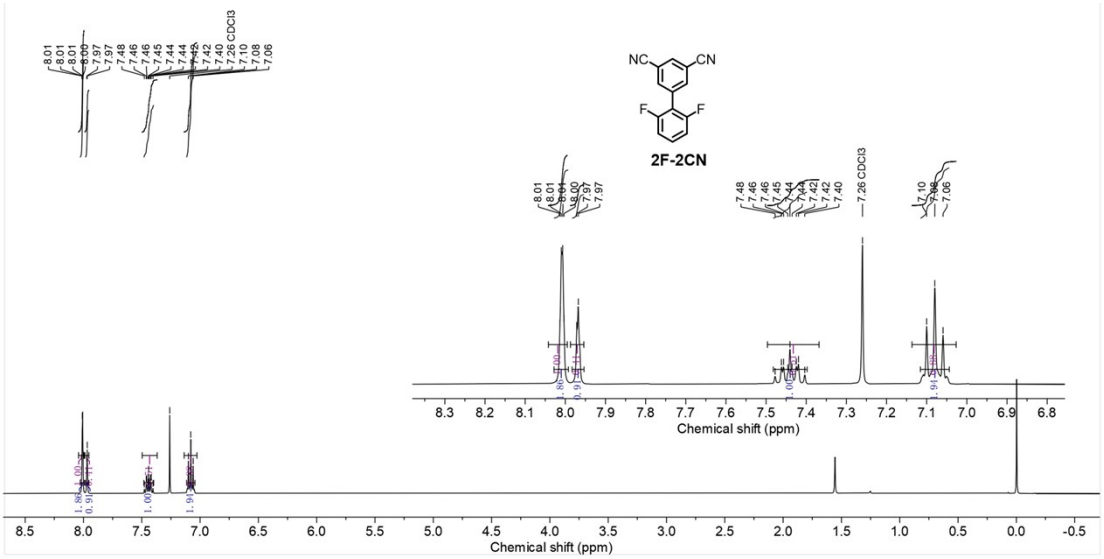

Fig. S2. ^{1}H NMR spectra of 2F-2CN in *d*-$CDCl_3$.

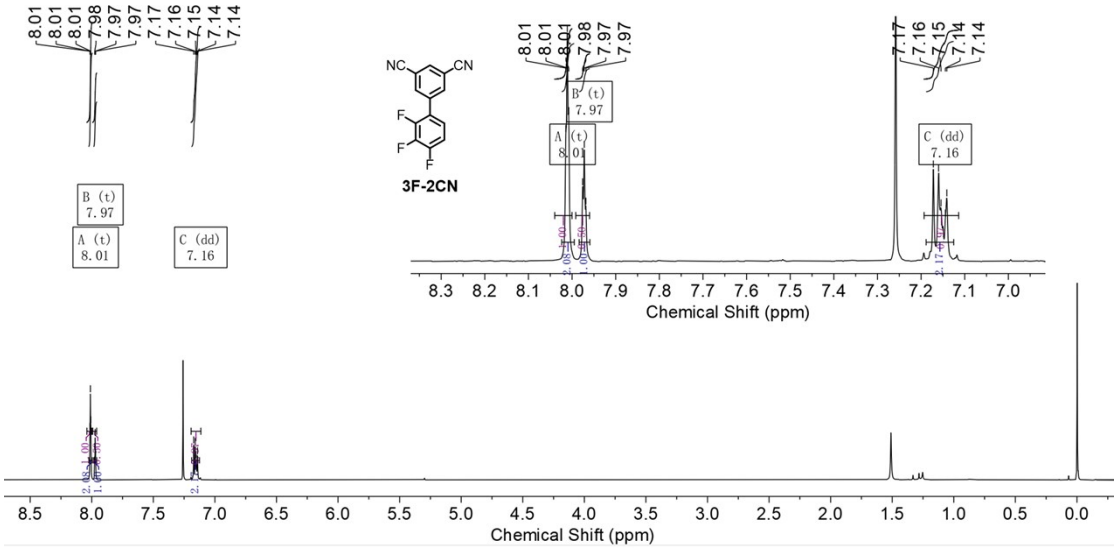

Fig. S3. ^{1}H NMR spectra of 3F-2CN in *d*-$CDCl_3$.

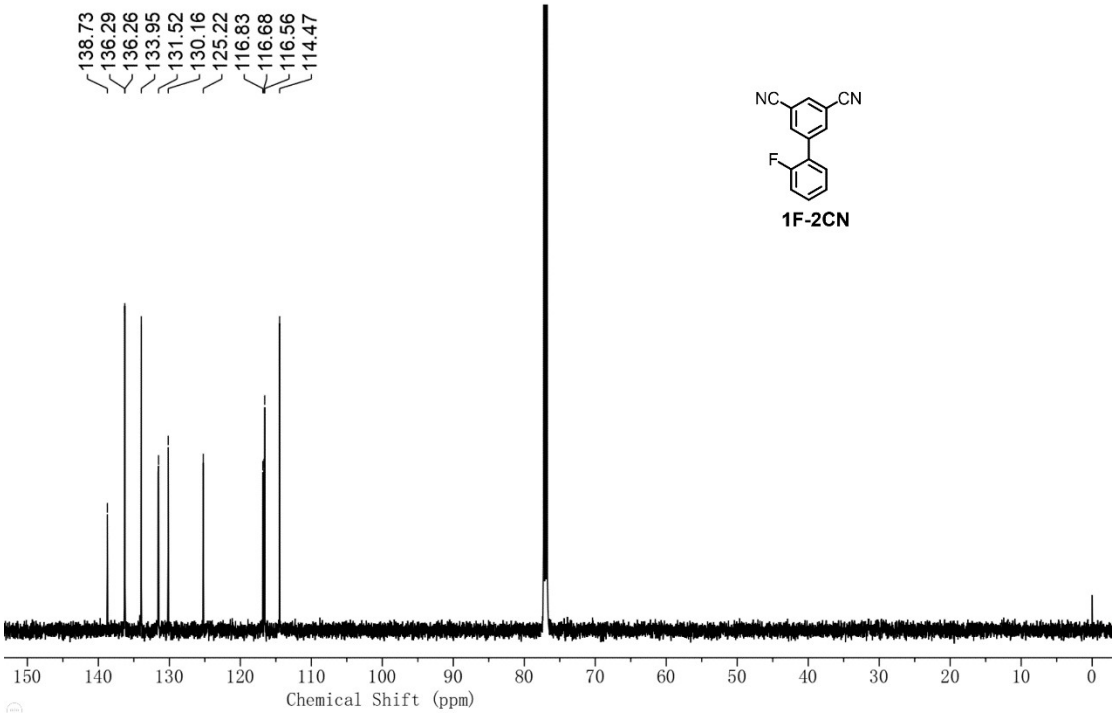

Fig. S4. ^{13}C NMR spectra of 1F-2CN in *d*-$CDCl_3$.

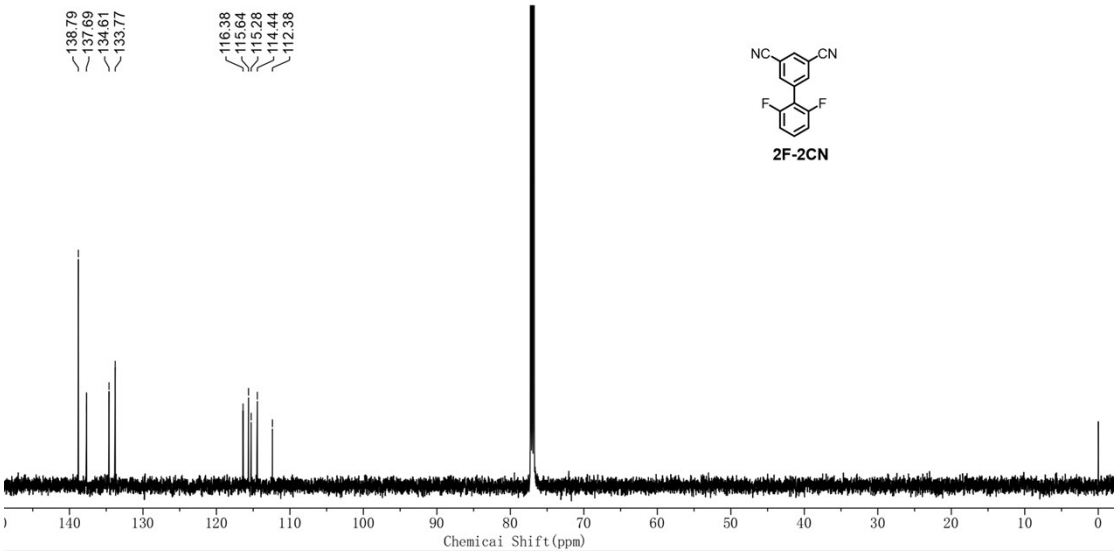

Fig. S5. ^{13}C NMR spectra of 2F-2CN in *d*-$CDCl_3$.

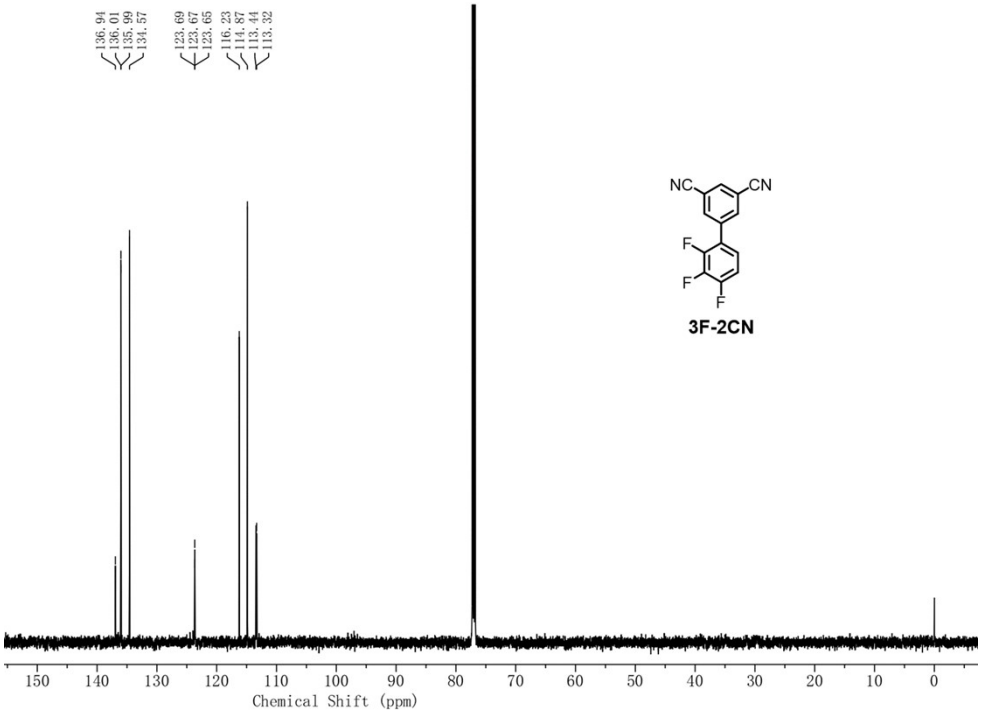

Fig. S6. ^{13}C NMR spectra of 3F-2CN in *d*-$CDCl_3$.

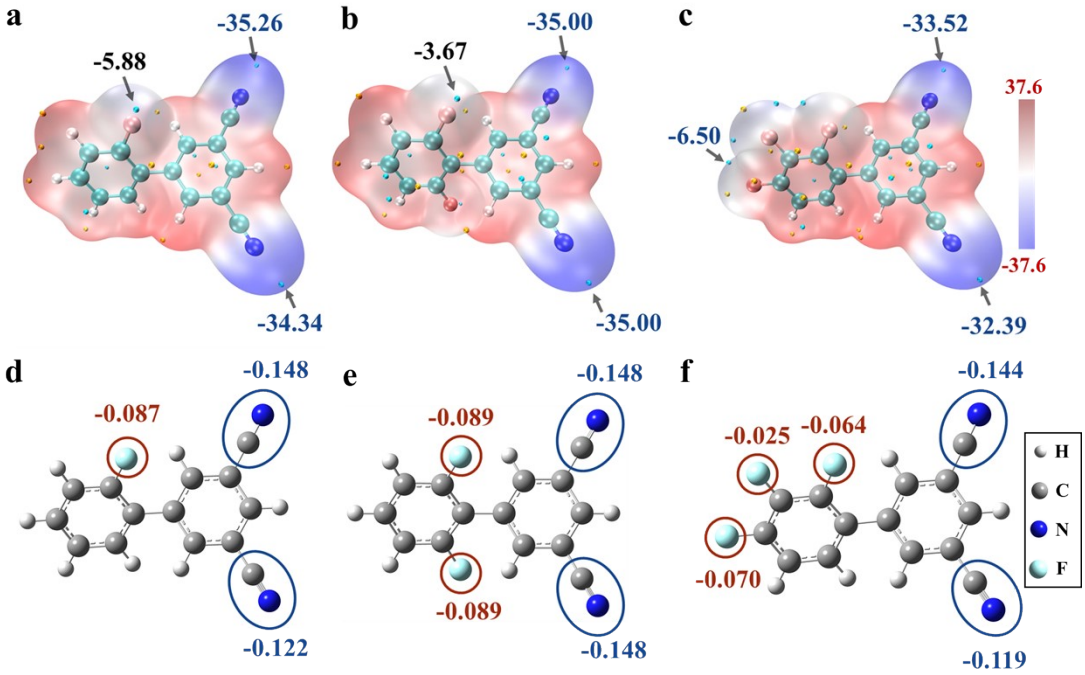

Fig. S7. The ESP maps of (a) 1F-2CN, (b) 2F-2CN and (c) 3F-2CN molecules (unit: kcal/mol). The fragment charge of (d) 1F-2CN, (e) 2F-2CN and (f) 3F-2CN molecules.

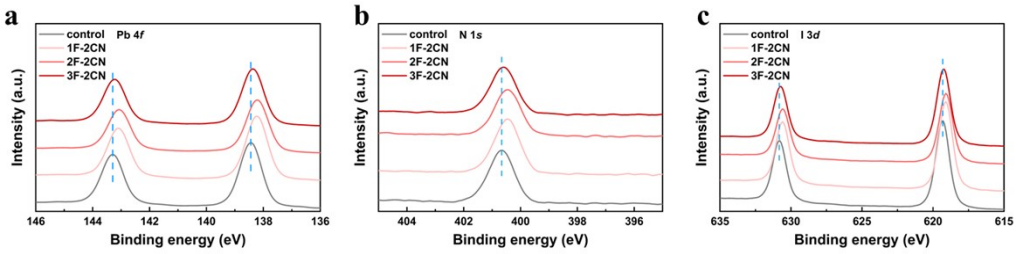

Fig. S8. The XPS spectra of perovskite films deposited on ITO glass corresponding to core levels of (a) Pb 4*f*, (b) N 1*s* and (c) I 3*d*.

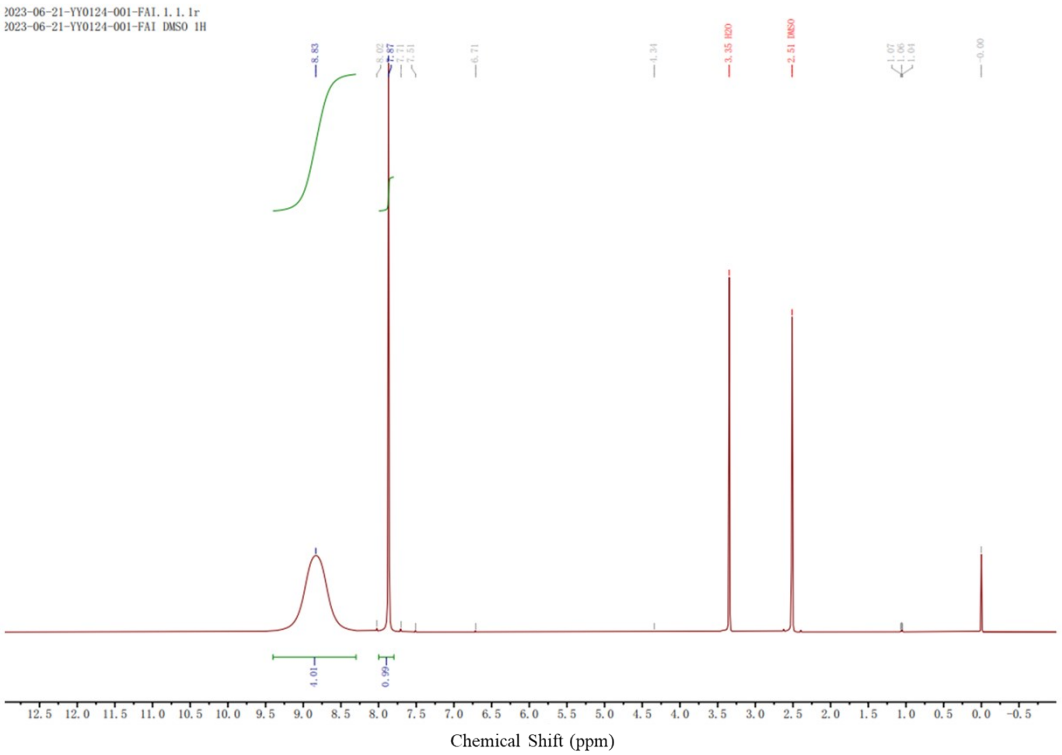

Fig. S9. [1]H NMR spectra of FAI in *d*-DMSO.

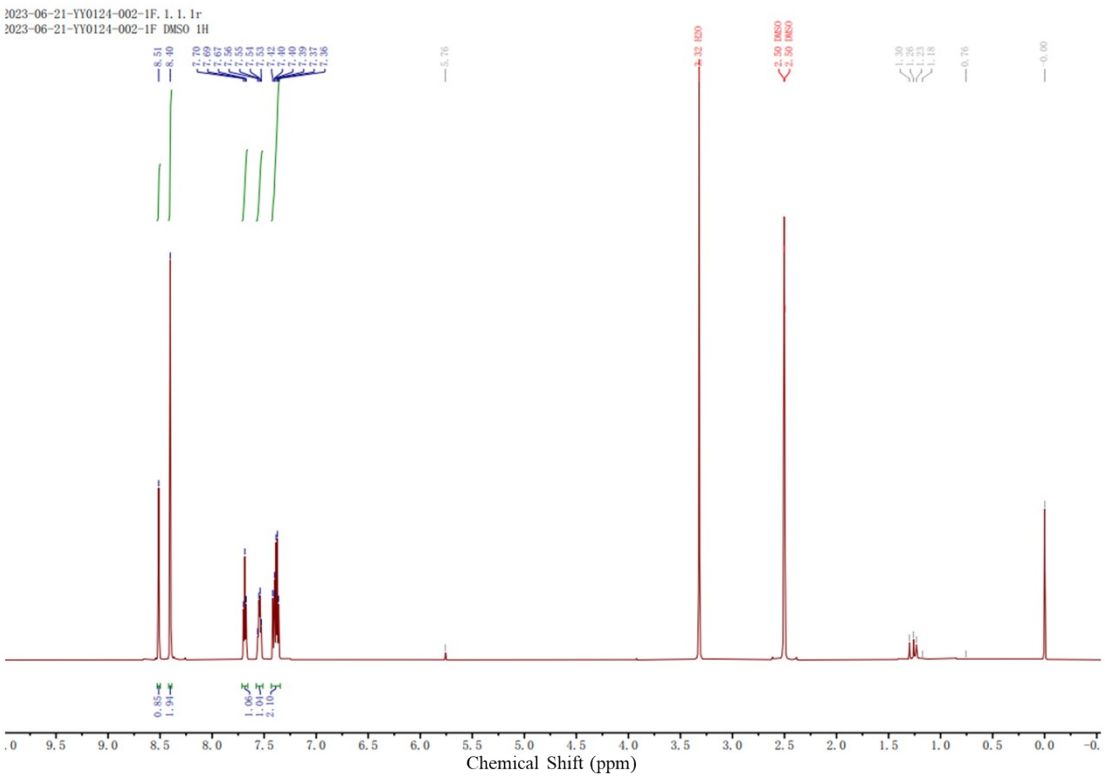

Fig. S10. [1]H NMR spectra of 1F-2CN in *d*-DMSO.

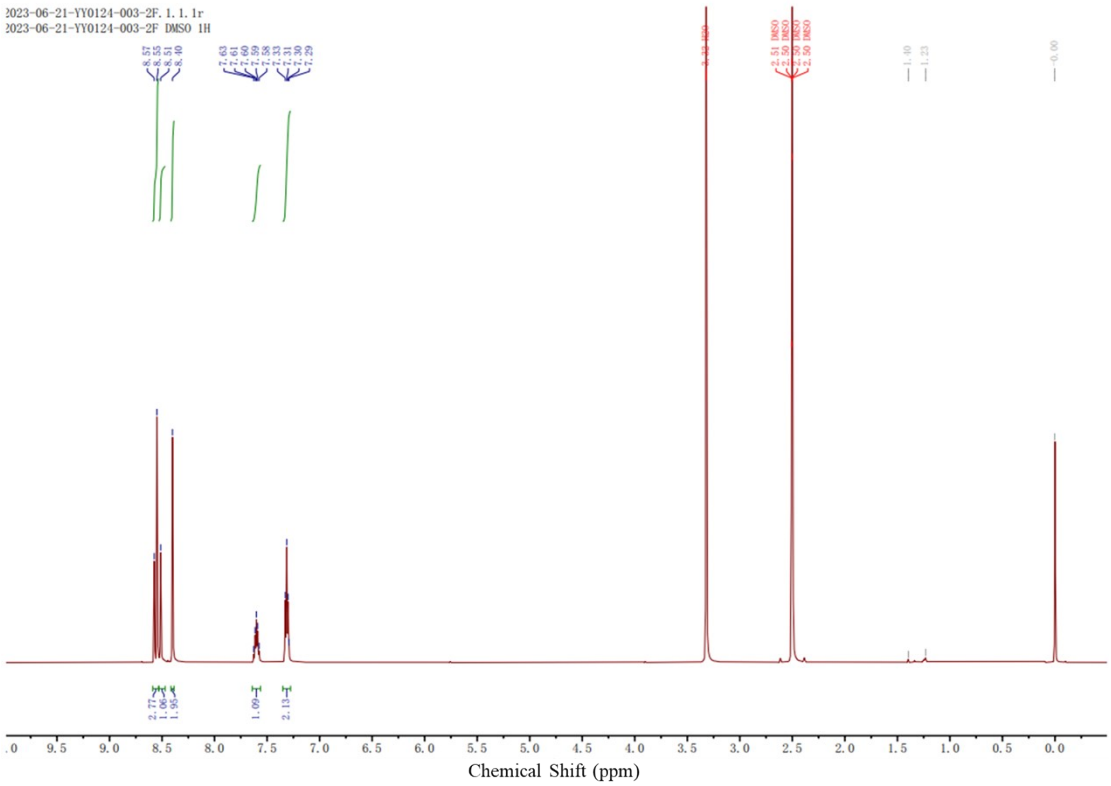

Fig. S11. [1]H NMR spectra of 2F-2CN in *d*-DMSO.

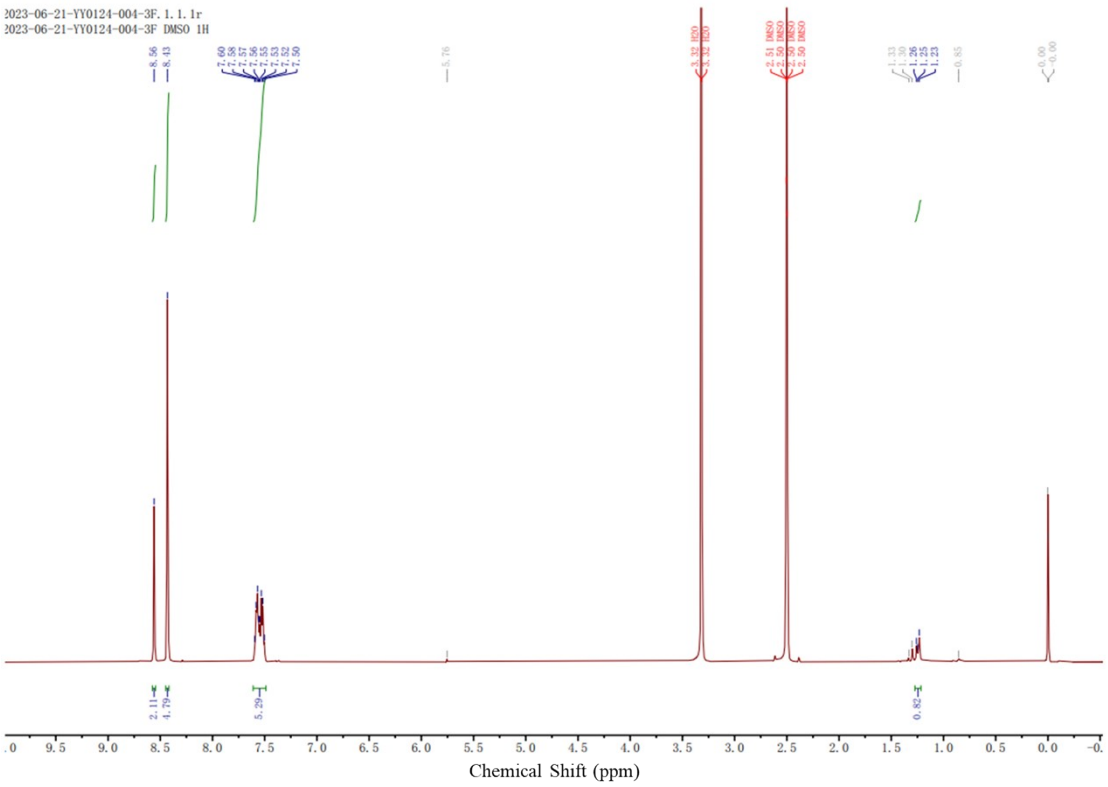

Fig. S12. [1]H NMR spectra of 3F-2CN in *d*-DMSO.

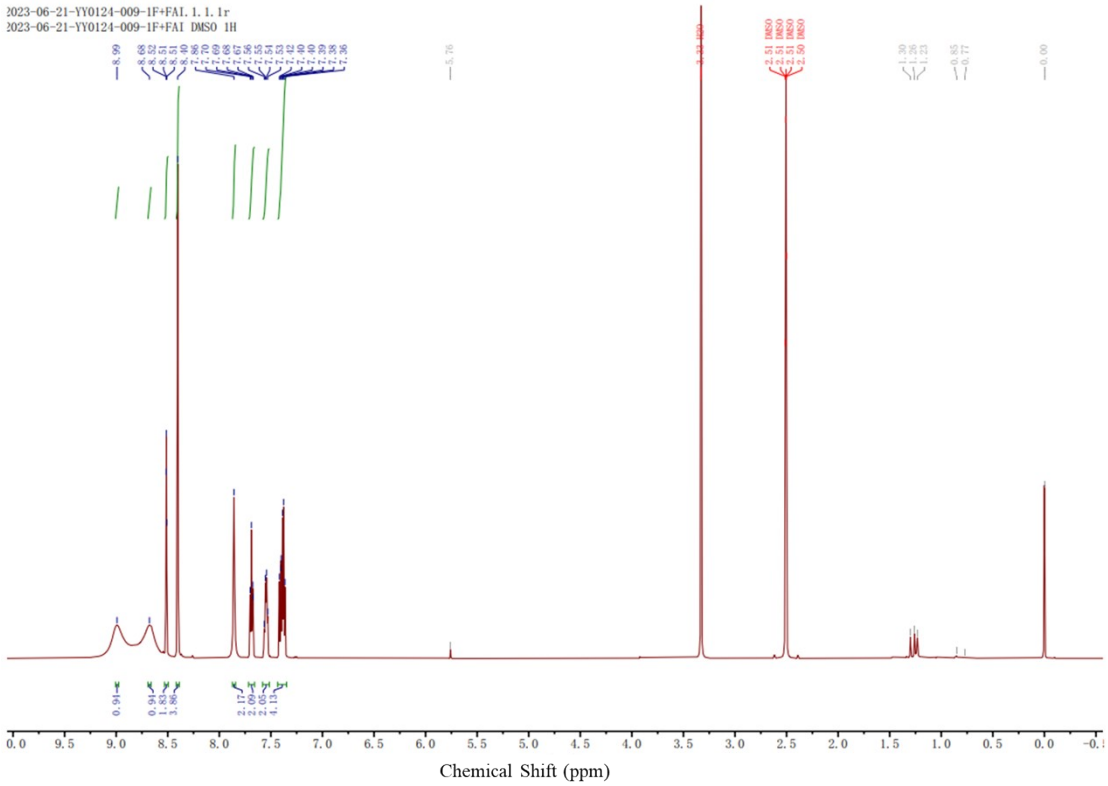

Fig. S13. [1]H NMR spectra of 1F-2CN/FAI in *d*-DMSO.

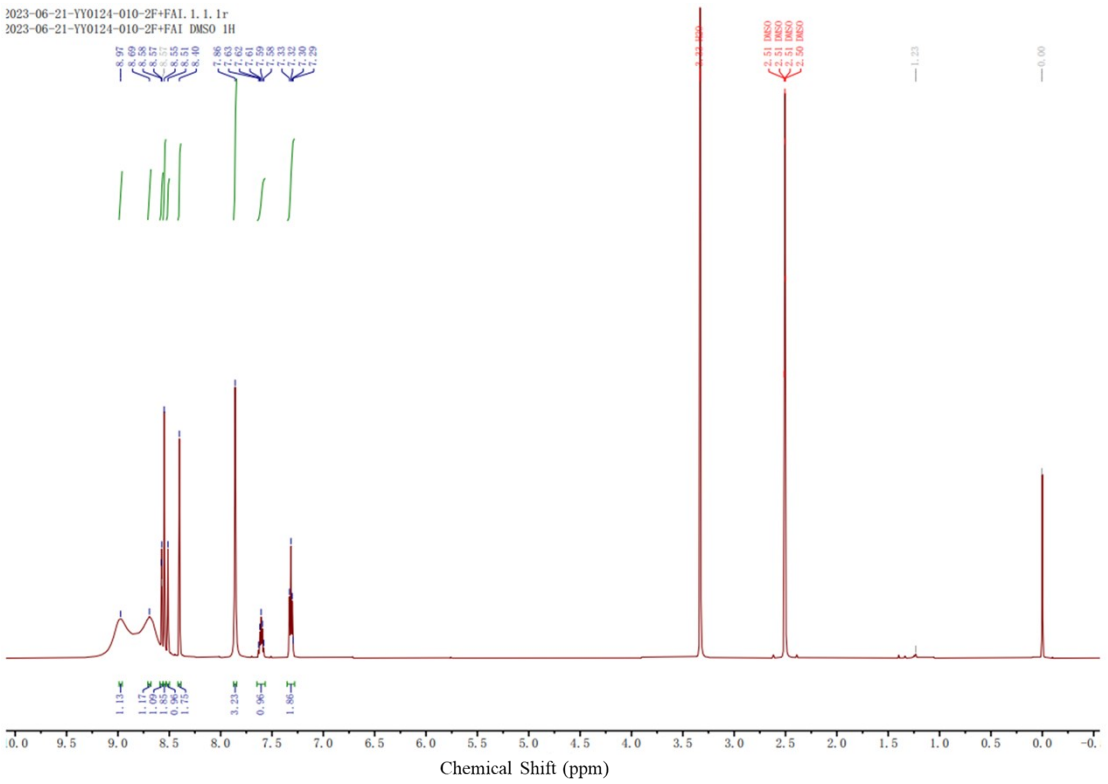

Fig. S14. [1]H NMR spectra of 2F-2CN/FAI in *d*-DMSO.

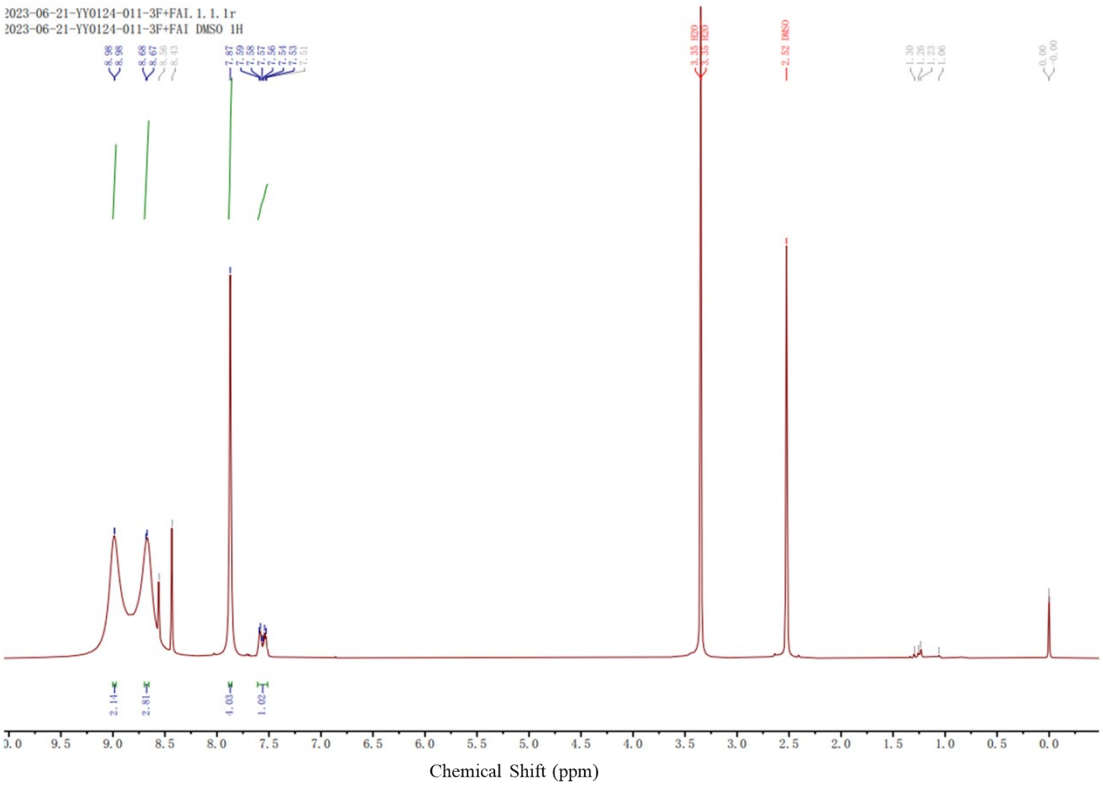

Fig. S15. ^{1}H NMR spectra of 3F-2CN/FAI in *d*-DMSO.

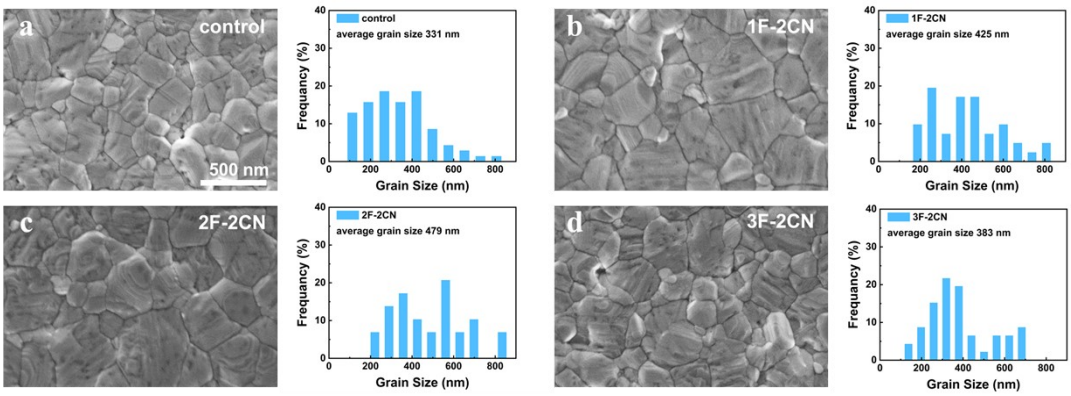

Fig. S16. Top-view SEM images and the corresponding grain size distributions of the (a) control, (b) 1F-2CN, (c) 2F-2CN, and (d) 3F-2CN modified perovskite films.

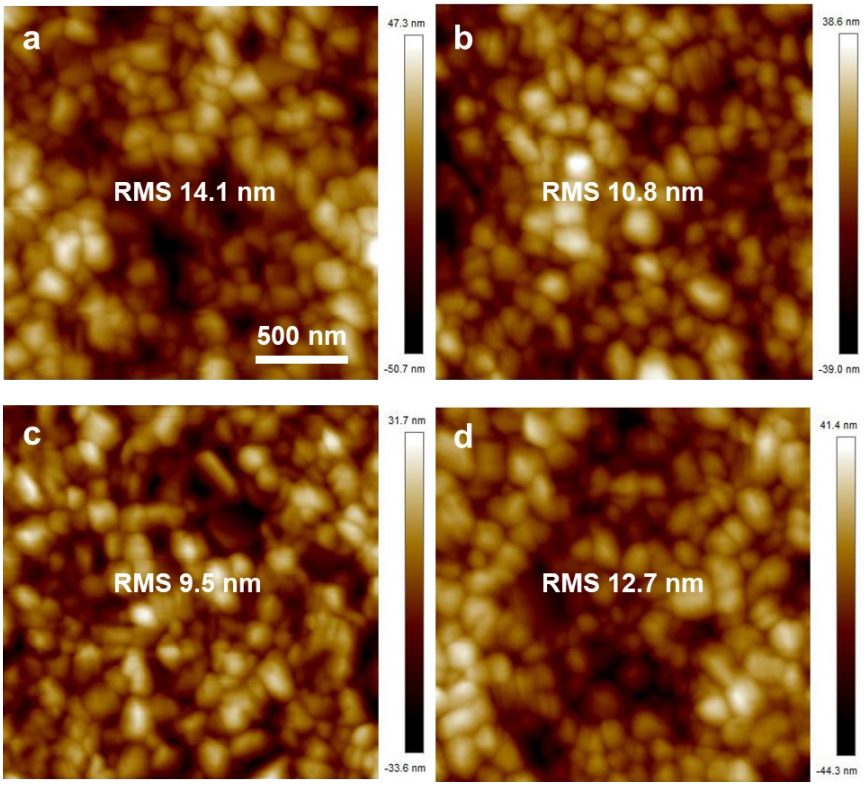

Fig. S17. AFM height images of the (a) control, (b) 1F-2CN, (c) 2F-2CN, and (d) 3F-2CN modified perovskite films.

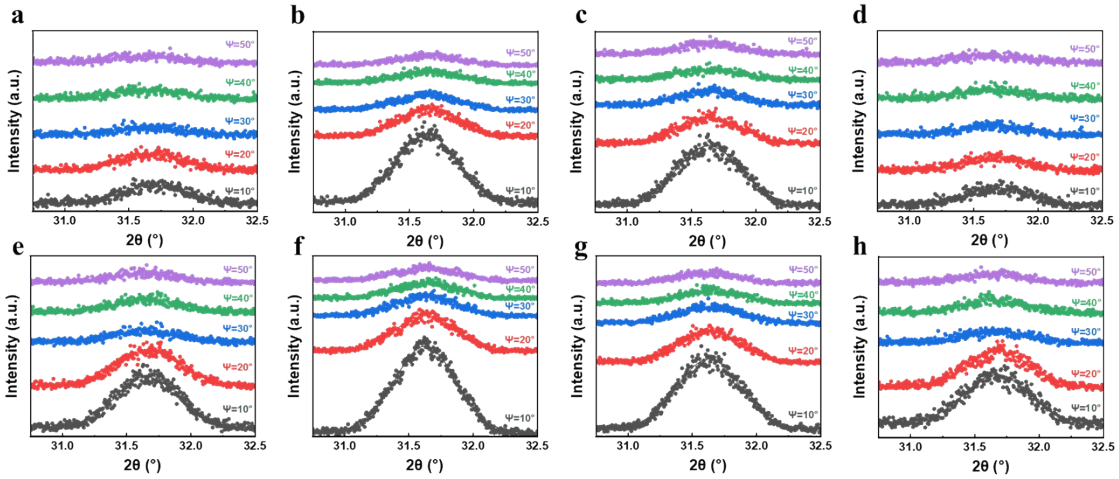

Fig. S18. GIXRD with different instrumental Ψ values of (a) control, (b) 1F-2CN, (c) 2F-2CN, and (d) 3F-2CN modified perovskite films, where the incident angle is 0.2°. GIXRD with different instrumental Ψ values of (e) control, (f) 1F-2CN, (g) 2F-2CN, and (h) 3F-2CN modified perovskite films, where the incident angle is 0.5°.

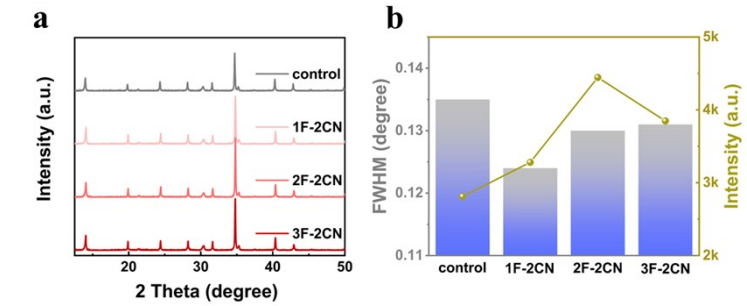

Fig. S19. (a) XRD patterns and (b) the corresponding FWHM/intensity of the perovskite films.

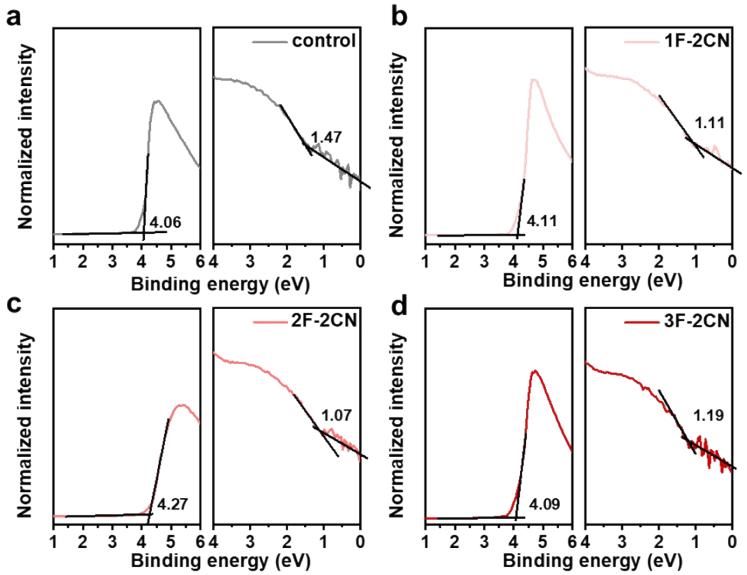

Fig. S20. UPS data of the (a) control, (b) 1F-2CN, (c) 2F-2CN, and (d) 3F-2CN modified perovskite films.

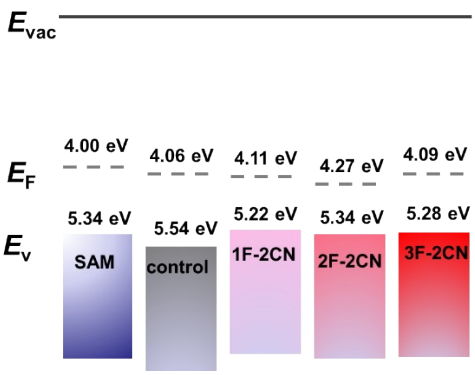

Fig. S21. Energy level scheme of the films. Vacuum level (E_{vac}), Valence band maximum (E_v), Fermi level (E_F) and [2-(3,6-dimethoxy-9H-carbazol-9-yl)ethyl] phosphonic acid (SAM).

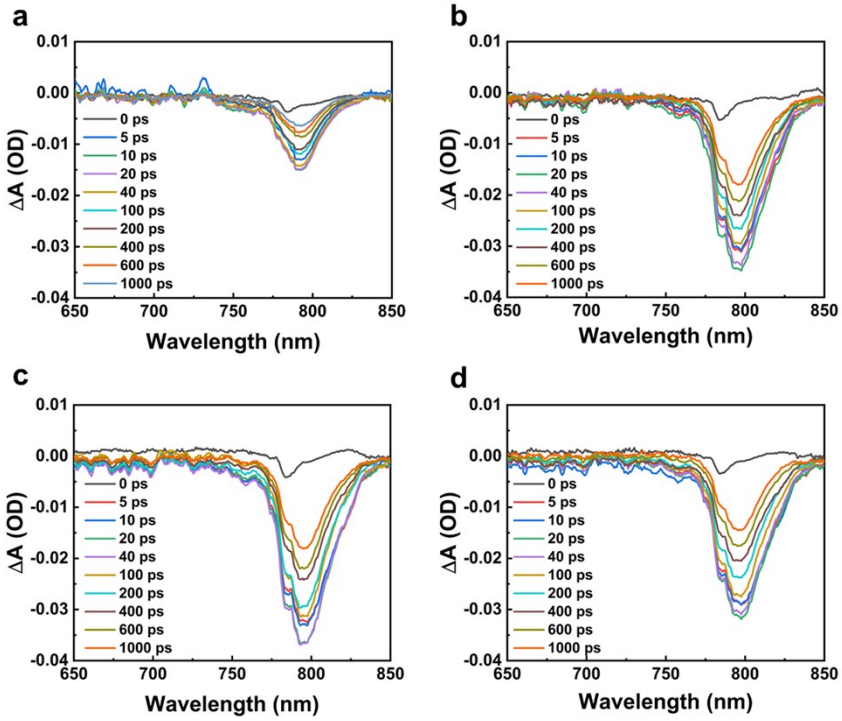

Fig. S22. TA spectra at different time delays of (a) control, (b) 1F-2CN, (c) 2F-2CN, and (d) 3F-2CN modified perovskite films.

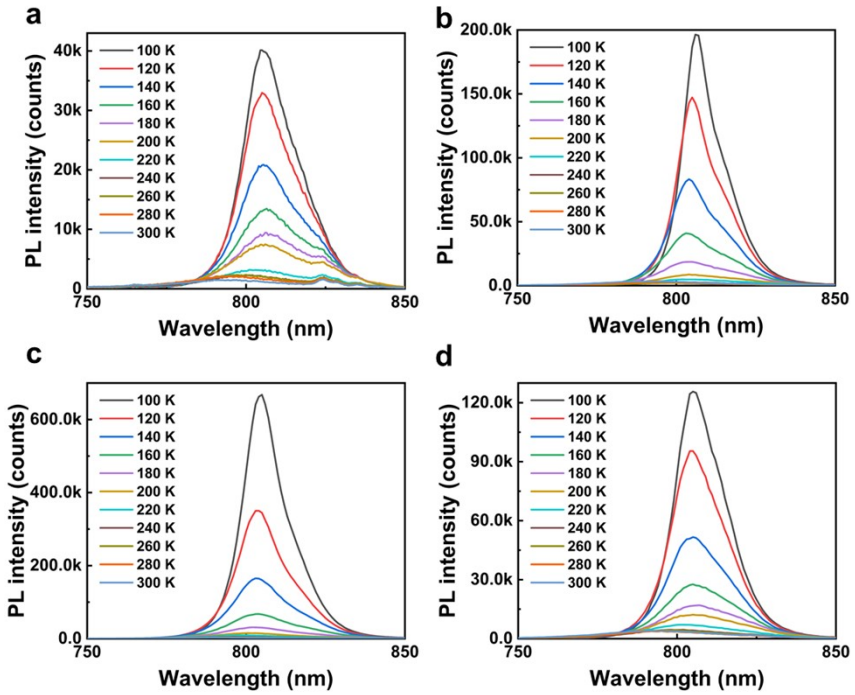

Fig. S23. Temperature-dependent PL spectra of (a) control, (b) 1F-2CN, (c) 2F-2CN, and (d) 3F-2CN modified perovskite films.

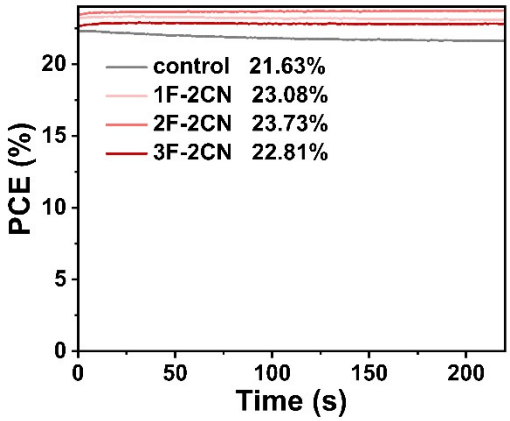

Fig. S24. SPO measurements of devices.

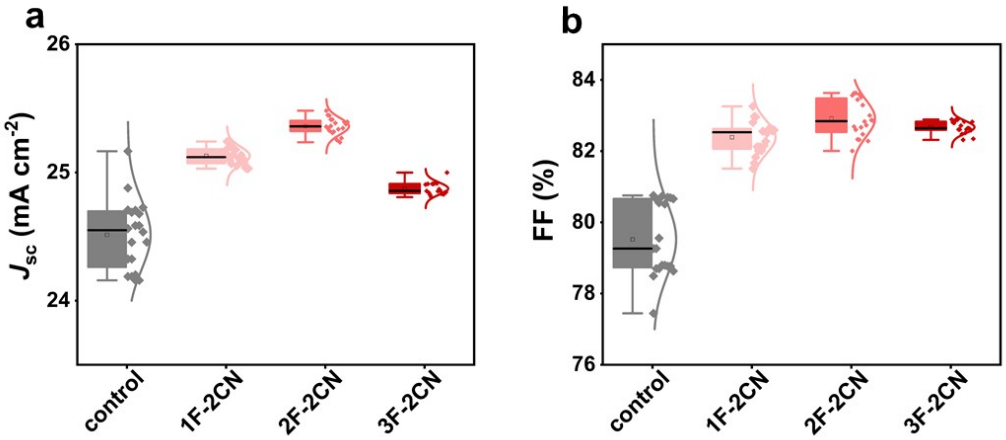

Fig. S25. Statistics of (a) J_{sc} and (b) FF for 20 devices.

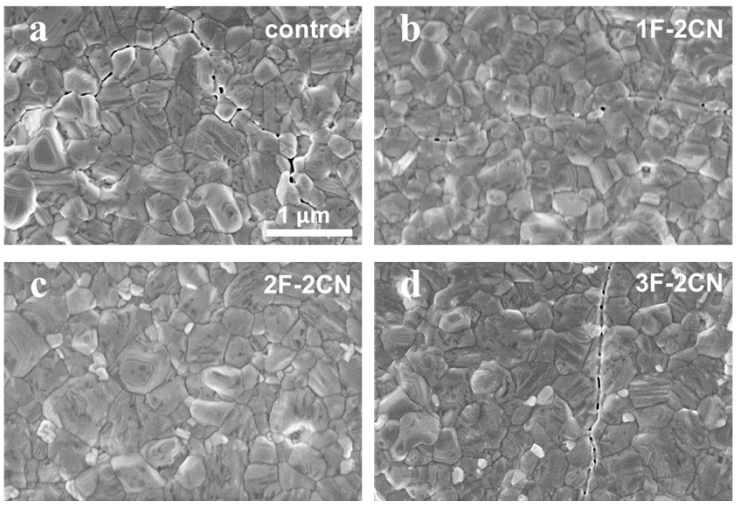

Fig. S26. Top-view SEM images of the (a) control, (b) 1F-2CN, (c) 2F-2CN, and (d) 3F-2CN modified perovskite films after 3000 cycles of bending. Magnification factor 50000 times.

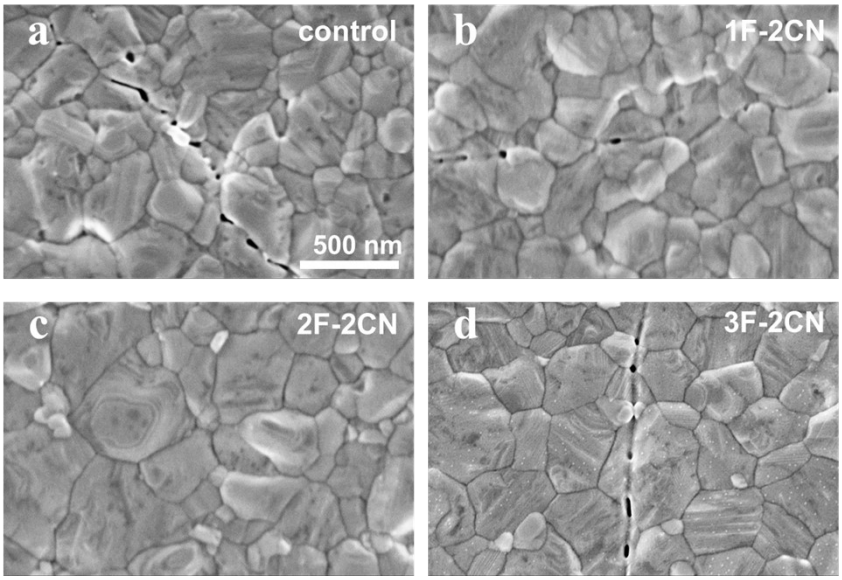

Fig. S27. Top-view SEM images of the (a) control, (b) 1F-2CN, (c) 2F-2CN, and (d) 3F-2CN modified perovskite films after 3000 cycles of bending. Magnification factor 80000 times.

Table S1 Performance summary of inverted f-PSCs.

Device Structure	J_{sc} (mA cm^{-2})	V_{oc} (V)	FF (%)	PCE (%)	Year
FTO/PEDOT:PSS/$CH_3NH_3PbI_{3-x}Clx$/$PC_{61}BM$/TiOx/Al	14.4	0.88	51	6.4	2013[10]
ITO/PEDOT:PSS/$CH_3NH_3PbI_3$/$PC_{61}BM$/bis-C_{60}/Ag	14.6	0.86	75	9.42	2014[11]
ITO/PEDOT:PSS/PEI·HI/$CH_3NH_3PbI_3$/$PC_{61}BM$/LiF/Ag	19.0	1.07	68	13.8	2015[12]
ITO/PEDOT:PSS/MoO_3/$CH_3NH_3PbI_3$/C_{60}/BCP/Ag	21.5	0.97	83	17.3	2016[13]
ITO/PTAA/FAMAPb(I_xBr_{1-x})$_3$/$PC_{61}BM$/C_{60}/BCP/Cu	22.8	1.06	75	18.1	2017[14]
TFSA-doped GR/PEDOT:PSS/$FAPbI_{3-x}Br_x$/$PC_{61}BM$/Al	22.1	1.07	77	18.3	2018[15]
ITO/PTAA/$CH_3NH_3PbI_3$-NH_4Cl/ C_{60}/BCP/Cu	22.8	1.09	79	19.72	2019[16]
ITO/NiO_x(F2HCNQ)/CsMAFAPbI_xBr_{3-x}/$PC_{61}BM$/BCP/Ag	22.2	1.12	81	20.01	2020[17]
ITO/PTAA/$Cs_{0.05}(FA_{0.98}MA_{0.02})_{0.95}Pb(I_{0.98}Br_{0.02})_3$/Organic BHJ/$Zr(acac)_4$/Ag	24.8	1.13	78	21.73	2021[18]
ITO/PTAA/PenAAc/$Cs_{0.05}(FA_{0.98}MA_{0.02})_{0.95}Pb(I_{0.98}Br_{0.02})_3$/$C_{60}$/BCP/Ag	24.8	1.17	81	23.68	2022[19]
ITO/DC-PA/$Cs_{0.05}(FA_{0.98}MA_{0.02})_{0.95}Pb(I_{0.98}Br_{0.02})_3$/$C_{60}$/BCP/Ag	24.1	1.19	81	23.23	2023[20]
ITO/MeO-2PACz/$Cs_{0.05}(FA_{0.98}MA_{0.02})_{0.95}Pb(I_{0.98}Br_{0.02})_3$/$C_{60}$/BCP/Ag	25.3	1.14	84	24.08	This work

Table S2 Fitted lifetimes for perovskite films from TRPL measurements.

Film	A_1	τ_1 (ns)	A_2	τ_2 (ns)	τ_a (ns)
control	109.67	6.20	59.87	236.57	226.02
1F-2CN	527.97	5.40	288.01	327.03	317.57
2F-2CN	551.80	4.27	249.00	346.97	337.88
3F-2CN	446.43	5.14	222.21	271.71	261.96

Table S3 Fitted lifetimes for perovskite films from TAS measurements.

Film	A_1	τ_1 (ps)	A_2	τ_2 (ps)	τ_a (ps)
control	-0.30	184.83	-0.55	1132.90	1056.58
1F-2CN	-0.28	141.23	-0.62	1531.64	1476.07
2F-2CN	-0.34	159.27	-0.73	2621.22	2554.32
3F-2CN	-0.29	175.46	-0.49	1334.97	1252.36

Table S4 Parameters derived via fitting the temperature-dependent FWHM.

Film	Γ_{inh} (meV)	Γ_{LO} (meV)	$h\omega$ (meV)
control	43	1429	842
1F-2CN	16	53	156
2F-2CN	3	26	81
3F-2CN	27	77	220

Table S5 The photovoltaic parameters for f-PSCs.

device	scan	J_{sc} (mA cm^{-2})	V_{oc} (V)	FF (%)	PCE (%)	HI (%)
control	reverse	24.88	1.105	79.56	21.87	2.01
	forward	24.52	1.097	78.10	21.01	
1F-2CN	reverse	25.18	1.134	82.80	23.64	0.20
	forward	25.10	1.131	82.96	23.54	
2F-2CN	reverse	25.36	1.136	83.57	24.08	0.21
	forward	25.31	1.133	83.59	23.98	
3F-2CN	reverse	24.91	1.129	82.89	23.30	0.23
	forward	24.82	1.127	82.89	23.20	

The *J-V* HI is defined by the equation: $$HI(\%) = \frac{PCE_{Reverse} - PCE_{Forward}}{PCE_{Reverse}}$$.

Table S6 The photovoltaic parameters for f-PSCs.

device	J_{sc} (mA cm^{-2})	V_{oc} (V)	FF (%)	PCE (%)
control	24.51±0.27	1.095±0.01	79.52±1.03	21.35±0.42
1F-2CN	25.13±0.07	1.131±0.01	82.39±0.46	23.42±0.11
2F-2CN	25.36±0.06	1.135±0.01	82.92±0.52	23.86±0.13
3F-2CN	24.87±0.05	1.126±0.01	82.67±0.17	23.15±0.07

1. H. Wang, C. Zhu, L. Liu, S. Ma, P. Liu, J. Wu, C. Shi, Q. Du, Y. Hao, S. Xiang, H. Chen, P. Chen, Y. Bai, H. Zhou, Y. Li and Q. Chen, *Adv. Mater.*, 2019, **31**, 1904408.
2. C. Zhu, X. Niu, Y. Fu, N. Li, C. Hu, Y. Chen, X. He, G. Na, P. Liu, H. Zai, Y. Ge, Y. Lu, X. Ke, Y. Bai, S. Yang, P. Chen, Y. Li, M. Sui, L. Zhang, H. Zhou and Q. Chen, *Nat. Commun.*, 2019, **10**, 815.
3. J. Li, L. Xie, Z. Pu, C. Liu, M. Yang, Y. Meng, B. Han, S. Bu, Y. Wang, X. Zhang, T. Wang and Z. Ge, *Adv. Funct. Mater.*, 2023, 2301956.
4. L. Xie, J. Liu, J. Li, C. Liu, Z. Pu, P. Xu, Y. Wang, Y. Meng, M. Yang and Z. Ge, *Adv. Mater.*, 2023, e2302752.
5. R. Su, Z. Xu, J. Wu, D. Luo, Q. Hu, W. Yang, X. Yang, R. Zhang, H. Yu, T. P. Russell, Q. Gong, W. Zhang and R. Zhu, *Nat. Commun.*, 2021, **12**, 2479.
6. H. Chen, Y. Wang, Y. Fan, Y. Chen, Y. Miao, Z. Qin, X. Wang, X. Liu, K. Zhu, F. Gao and Y. Zhao, *Natl. Sci. Rev.*, 2022, **9**, nwac127.
7. X. Yang, Y. Fu, R. Su, Y. Zheng, Y. Zhang, W. Yang, M. Yu, P. Chen, Y. Wang, J. Wu, D. Luo, Y. Tu, L. Zhao, Q. Gong and R. Zhu, *Adv. Mater.*, 2020, **32**, 2002585.
8. Y. Meng, C. Liu, R. Cao, J. Zhang, L. Xie, M. Yang, L. Xie, Y. Wang, X. Yin, C. Liu and Z. Ge, *Adv. Funct. Mater.*, 2023, 2214788.
9. L. Xie, X. Zhao, J. Wang, J. Li, C. Liu, S. Wang, Q. Bao, M. Yang, X. Niu, F. Hao and Z. Ge, *INFOMAT*, 2023, **5**, e12379.
10. P. Docampo, J. M. Ball, M. Darwich, G. E. Eperon and H. J. Snaith, *Nat. Commun.*, 2013, **4**, 2761.
11. J. W. Jung, S. T. Williams and A. K. Y. Jen, *RSC Adv.*, 2014, **4**, 62971-62977.
12. K. Yao, X. Wang, Y.-x. Xu and F. Li, *Nano Energy*, 2015, **18**, 165-175.
13. J. Yoon, H. Sung, G. Lee, W. Cho, N. Ahn, H. S. Jung and M. Choi, *Energy Environ. Sci.*, 2016, **10**, 337-345.
14. C. Bi, B. Chen, H. Wei, S. DeLuca and J. Huang, *Adv. Mater.*, 2017, **29**, 1605900.
15. J. H. Heo, D. H. Shin, D. H. Song, D. H. Kim, S. J. Lee and S. H. Im, *J. Mater. Chem. A*, 2018, **6**, 8251-8258.
16. X. Dai, Y. Deng, C. H. Van Brackle, S. Chen, P. N. Rudd, X. Xiao, Y. Lin, B. Chen and J. Huang, *Adv. Energy Mater.* , 2020, **10**, 1903108.
17. P. Ru, E. Bi, Y. Zhang, Y. Wang, W. Kong, Y. Sha, W. Tang, P. Zhang, Y. Wu, W. Chen, X. Yang, H. Chen and L. Han, *Adv. Energy Mater.* , 2020, **10**, 1903487.
18. S. Wu, Z. Li, J. Zhang, X. Wu, X. Deng, Y. Liu, J. Zhou, C. Zhi, X. Yu, W. C. H. Choy, Z. Zhu and A. K. Y. Jen, *Adv. Mater.*, 2021, **33**, 2105539.
19. D. Gao, B. Li, Z. Li, X. Wu, S. Zhang, D. Zhao, X. Jiang, C. Zhang, Y. Wang, Z. Li, N. Li, S. Xiao, W. C. H. Choy, A. K. Y. Jen, S. Yang and Z. Zhu, *Adv. Mater.*, 2023, **35**, 2206387.
20. S. Wu, J. Zhang, M. Qin, F. Li, X. Deng, X. Lu, W.-J. Li and A. K. Y. Jen, *Small*, 2023, 2207189.